JOURNAL OF MATERIALS SCIENCE **35** (2000) 1219–1230

# Relationship between morphology and mechanical properties of polypropylene/ethene-co-butene binary blends with various butene contents

D. E. MOUZAKIS
*Institut für Verbundwerkstoffe GmbH, Universität Kaiserslautern, Pf. 3049, D-67663 Kaiserslautern , Germany*

D. MÄDER[#], R. MÜLHAUPT
*Freiburger Materialforschungszentrum, Albert-Ludwigs-Universität, Stefan-Meier-Str. 21, D-79104 Freiburg, Germany*

J. KARGER-KOCSIS[*]
*Institut für Verbundwerkstoffe GmbH, Universität Kaiserslautern, Pf. 3049, D-67663 Kaiserslautern, Germany*
*E-mail: karger@ivw.uni-kl.de*

A metallocene-based isotactic polypropylene (m-iPP) was blended with various types of ethene-co-butene rubbers (EBR). Blend miscibility was examined by means of dynamic mechanical analysis (DMTA). In addition, morphology was studied on cyclohexane etched cryofractured samples. Stiffness and toughness properties were assessed and interpreted in function of the blend miscibility. Izod tests served for the dynamic fracture toughness characterization. The essential work of fracture (EWF) approach was used for the characterization of the static fracture toughness. It was found that the 1-butene content of the EBR strongly affects the blend miscibility. A disperse structure was found as prerequisite for outstanding overall toughness. When distiguishing between resistance to crack initiation and propagation, it was found that they are changing adversely to one another. 

## 1. Introduction

Isotactic polypropylene (iPP) is used in a wide range of applications due to the attractive properties of relative high stiffness, heat distortion temperature including its low price. However, the impact toughness of iPP is relatively low especially at subambient temperatures. The toughness is often being improved by melt blending with various elastomers [1] or by copolymerization [2]. This is, however, associated with reduction in stiffness and strength and therefore various fillers are often incorporated in order to compensate this effect.

Thermoplastic elastomers such as styrene/ethene-co-1-butene/styrene (SEBS), have shown to exhibit an attractive prospect to improve toughness without a dramatic loss in stiffness. The authors have already studied these systems in previous works [3, 4].

The progress in metallocene catalysis has expanded the availability of tailor-made polyolefin copolymers [5]. In a recent study [6] it was shown that metallocene-based ethene/1-butene rubbers (EBR's) have the potential to act as effective impact-modifiers for iPP. It has been established that EBR's rich in 1-butene are miscible in the melt phase with iPP [7–10].

This work focuses on the relationship between stiffness, strength and toughness as a function of the rubber volume fraction of the polymer blends composed of a special type of metallocene-based i-PP matrix and various types of EBR rubbers. For the toughness assessment the essential work of fracture approach (EWF) was adopted due to its experimental simplicity and the very wide applicability window for these ductile systems. The dynamic fracture response was derived from Izod impact tests.

## 2. Materials

iPP used in this study was a novel metallocene-polymerized type (m-iPP), Novolen M®, from BASF AG. Poly(ethene-*co*-1-butene)s (EBR's) were prepared using methylaluminoxane-activated metallocene rac-$Me_2Si$(2-MeBenz [e] Ind)$_2ZrCl_2$ (MBI), as described in detail elsewhere [9].

[*] Author to whom all correspondence should be addressed.
[#] Present address: Ciba Speciality Chemicals Inc., CH-4002 Basel, Switzerland.

TABLE I Physical properties of the poly(ethene-co-1-butene) polymers (EBR) and metallocene-synthesized isotactic polypropylene (m-iPP)

| Polymer | EBR48 | EBR58 | EBR62 | EBR82 | EBR90 | m-iPP |
|---|---|---|---|---|---|---|
| EB 1-butene content | 48 | 58 | 62 | 82 | 90 | — |
| Ethene content[a] (mol%) | 68.9 | 58.8 | 54.1 | 30.1 | 19.0 | — |
| 1-butene content[a] (mol%) | 31.1 | 41.2 | 44.9 | 69.9 | 81.0 | — |
| Ethene content[a] (wt%) | 52.1 | 41.7 | 38.0 | 17.7 | 10.5 | — |
| 1-butene content[a] (wt%) | 47.1 | 58.3 | 62.0 | 82.3 | 89.5 | — |
| $M_n$ (kg/mol)[b] | 60.8 | 48.2 | 65.6 | 40.5 | 73.9 | 117.0 |
| $M_w/M_n$[b] | 2.2 | 2.7 | 2.2 | 2.2 | 2.2 | 2.2 |
| Glass transition temperature, $T_g$ (°C)[d/c] | −55/−60.1 | −56/−60.5 | −52/−57.1 | −32/−41.9 | −27/−37.7 | 5/0 |
| Melting temperature, $T_m$ (°C)[c] | — | — | — | 41.2 | 56.7 | 149.5 |
| Melt enthalpy, $\Delta H_m$ (J/g)[c] | — | — | — | 15.5 | 26.7 | 84.5 |
| Crystallization temperature, $T_{cr}$ (°C) | — | — | — | — | — | 113 |

[a]Determined by $^1$H-NMR.
[b]Determined by means of high-temperature GPC based on poly(ethene) standards.
[c]Determined by DSC at a heating rate of 10 °C min.
[d]Determined by dynamic mechanical analysis at a heating rate of 2 °C/min.
— Could not be detected.

m-iPP was melt blended with five different EBR's with varying 1-butene weight fraction in EBR. The molecular characteristics of the polymers used are given in Table I. The numbers denote the approximate weight fraction in EBR. The EBR48, −58 and −62 types are completely amorphous as evidenced by wide angle x-ray scattering (WAXS) and differential scanning calorimetry (DSC). On the other hand, the EBR82 and EBR90 types exhibit inherent crystallinity and thus show some similarity with poly(1-butene). It can be predicted that the difference in EBR crystallinity affects the stiffness, strength and toughness properties of these blends.

Each of the EBR's was blended in volume fractions of 5, 10, 15 and 20% respectively, with the aforementioned m-iPP.

### 2.1. Specimen preparation-melt blending

Melt blends were prepared using a Haake Rheomix 90 twin-screw kneader equipped with a 60 mL mixing chamber which was preheated at 200 °C and operated at 60 rpm. The chamber was always charged with 45 mL of polymer. m-iPP was molten in the presence of stabilizers (0.5 wt % Irganox® 1010/Irgafos® 168; 80 wt%/20 wt%, both of Ciba Specialty Chemicals) for 1.5 min. Then the EBR was added within 30 s. After another 3 min (total mixing time was 5 min) the sample was quickly recovered and quenched between cooled metal plates. Sheets of various in thicknesses were prepared by compression molding: the sample was heated at 200 °C for 10 min in a press (Schwabenthan Polystat 100) and quenched to ambient temperature by water-cooling [6].

## 3. Experimental

### 3.1. Viscoelastic behaviour

The thermomechanical properties and miscibility of the blends were studied by means of dynamic thermal and mechanical analysis (DMTA). An Eplexor™ 150 N (Gabo Qualimeter, Ahlden, Germany) DMTA machine has been employed to carry out this type of tests. Rectangular specimens of $60 \times 10 \times 1$ mm (length × width × thickness) were subjected to tensile dynamic loading consisting of a static preload of $6 \pm 0.2$ N on which a sinusoidal wave of $3 \pm 0.1$ N at 10 Hz frequency was superimposed. Heating occurred at a rate of 1 C°/min and in a temperature range between −100 and 150 °C.

### 3.2. Stiffness-strength

Tensile properties were measured on an Instron (Model 4202) tensile machine according to the DIN 53455 standard procedure using test specimens of 2 mm thickness and a crosshead speed of 10 mm/min. The average standard deviations of the Young's modulus and yield stress were approximately 5%. A minimum of five specimens was tested for each blend composition and the average value is reported. All tests were performed at ambient temperature ($25 \pm 2$ °C).

### 3.3. Fracture toughness

Notched Izod impact strength values were determined on notched samples according to ISO 180/1A using test specimens of $60 \times 10 \times 4$ mm$^3$.

Deeply double edge notched tensile (DDEN-T) specimens were used for the static fracture tests. Rectangular specimens of $85 \times 25$ mm$^2$ were cut by using a table saw of the compression molded plates of 1 mm thickness (cf. Fig. 1). Notching was performed by a bandsaw and specimens were consequently precracked by tapping with a razor blade. Tensile tests were performed on a Zwick™ 1445 1 kN (Ulm, Germany) universal testing machine equipped with mechanical extensometres, at a crosshead speed of 1 mm/min.

### 3.4. Essential work of fracture

For the plastic fracture analysis of the PP/EBR binary blends the essential work of fracture (EWF) approach was adopted. According to the EWF theory [11–13], a distinction is being made between a process zone or process plane where the actual crack runs and a plastic zone, which surrounds the process zone. In the plastic zone various processes take place, such as cavitation,

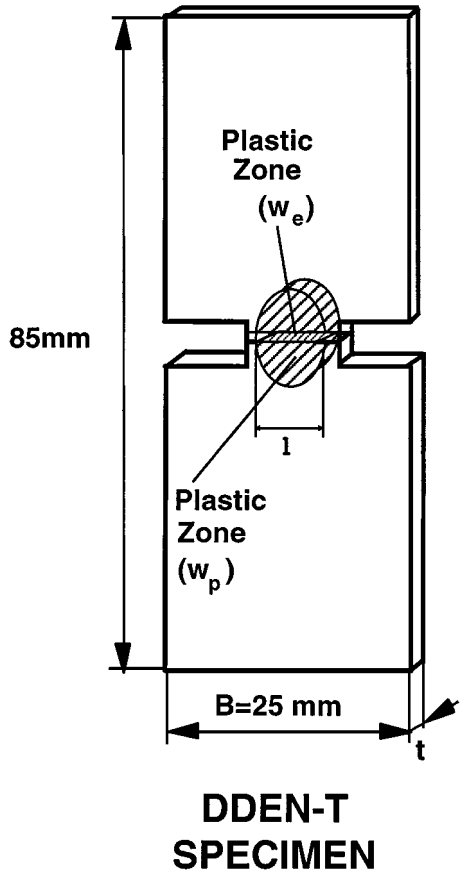


*Figure 1* DDENT specimen.

crazing, shear yielding etc. Consequently, the total work required to fracture a pre-cracked specimen can also be divided in two parts associated with each of the two zones mentioned above. Therefore we can write:

$$W_f = W_e + W_p \tag{1}$$

where $W_f$ is the total fracture work, $W_e$ the work spent for the crack advance in the crack plane and thus the generation of new surfaces and $W_p$ the energy consumed in the plastic zone by the dissipating mechanisms. Obviously, $W_e$ is related with a 2-D plane and is therefore a function of area ($lt$) whereas $W_p$ is dissipated in a 3-D zone and can be thus considered a function of volume ($l^2t$),where: $t =$ specimen thickness, $l =$ ligament width. Accordingly, Equation 1 can be expressed by the specific terms:

$$w_f = w_e + \beta w_p l \tag{2}$$

where: $w_f = W_f/lt$, $w_p = W_p/l^2t$, and $\beta$ is a geometry factor associated with the shape of the plastic zone.

According to Equation 2 the work of fracture is a linear function of the ligament size. $w_f$ can be plotted against ligament ($l$) for all specimens then $w_e$ can then be determined from the interception of the linear regression line with the $y$-axis [14]. It should be mentioned here that the total work of fracture $W_f$ can be determined by calculating the integral of force over time from the tensile tests up-to-rupture of deeply double edge notched tensile (DDEN-T, cf. Fig. 1) specimens of increasing ligaments. A very important prerequisite of the EWF method is that crack propagates only after the ligament has been fully yielded. In the blends studied, this indeed has always been the case as can be seen in Fig. 2, on the example of the m-iPP/EBR48 (95 vol. %/ 5 vol. %) blend. Pictures were taken by means of a travelling light microscope at back face illumination. Fig. 2 shows that the ligament region yields gradually, prior to the crack propagation. Pictures a and b in Fig. 2 show that there is no visible change on the specimen surface until the end of the elastic regime. The crack tips blunt and the ligament zone fully yields afterwards as pictures c and d show. The ligament region undergoes full plastic yielding and necking which is marked by a significant load drop; see frame d in Fig. 2. The almost linear reduction of load is typical for a stable crack growth, as seen in frame e. Finally, (frame f in Fig. 2) both cracks meet each other at the ligament center and ultimate rupture occurs.

### 3.5. Morphology characterization

In order to elucidate the actual morphology of each of the m-iPP/EBR blends in terms of miscibility, cyclohexane etched cryofractured samples were investigated by scanning electron microscopy (SEM). Small rectangular specimens of the 20 vol.% rubber fraction of each blend were dipped in liquid nitrogen for about 1 min and were fractured afterwards by using an impact pendulum. The cryofractured specimens were stored in cyclohexane for about 72 hours 20 °C. Cyclohexane is known to be a very good selective solvent for the elastomer in PP blends [15]. SEM pictures were taken from the etched fracture surfaces after gold sputtering.

### 3.6. Failure mode

Process zone (i.e. fracture zone) surfaces of the DDENT specimens and also those of the cryogenically fractured and etched specimens were examined with a JEOL™ JSM 5400 scanning electron microscope. Prior to investigation, specimens were sputtered with a Pt/Pd alloy.

## 4. Results and discussion

### 4.1. Microstructure

DMTA tests delivered interesting results of the microstructure and viscoelastic character of the various PP/EBR blends. It is well known from the related theory [16] that in case of incompatible blends, the glass transition ($T_g$) peaks of the constituents are well discernible. On the other hand, compatible polymer blends are characterized by a single $T_g$. In partially miscible systems, $T_g$'s shift towards each other.

By DMTA testing it was proved that three out of the six polymer blends are miscible, presenting only one $T_g$ or $\beta$-relaxation (EBR62, 82, 90) whereas in the other two (EBR48, −58), two relaxation domains namely $\beta_1$ and $\beta_2$ could be well resolved. $\beta_2$ relaxation was assigned to the elastomer component $T_g$, whereas $\beta_1$ was attributed to the $T_g$ of the amorphous PP. Due to this effect, the PP/EBR blends will be referred to as miscible

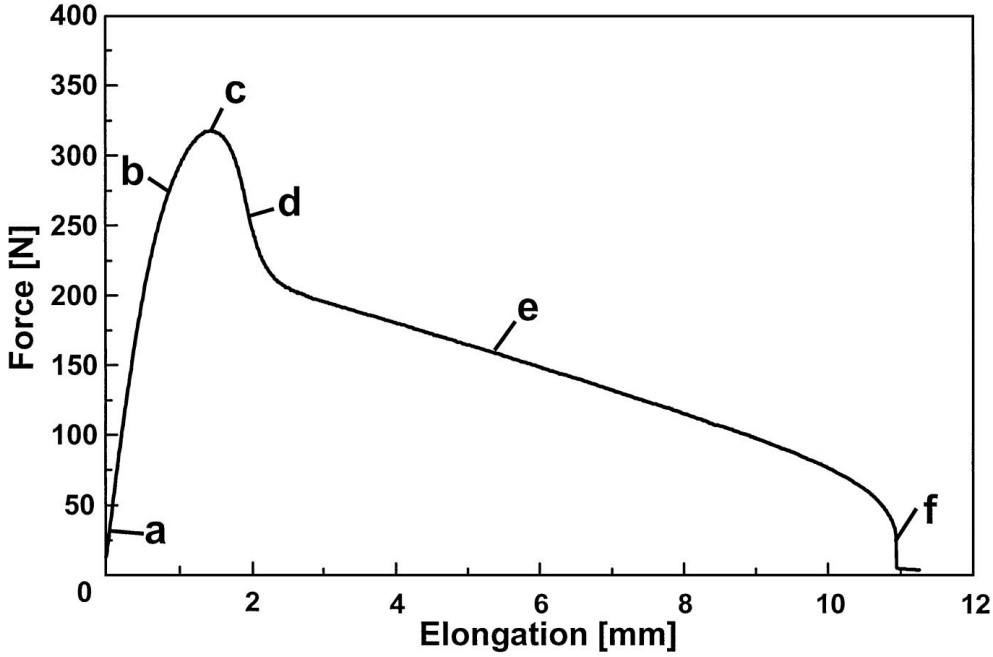


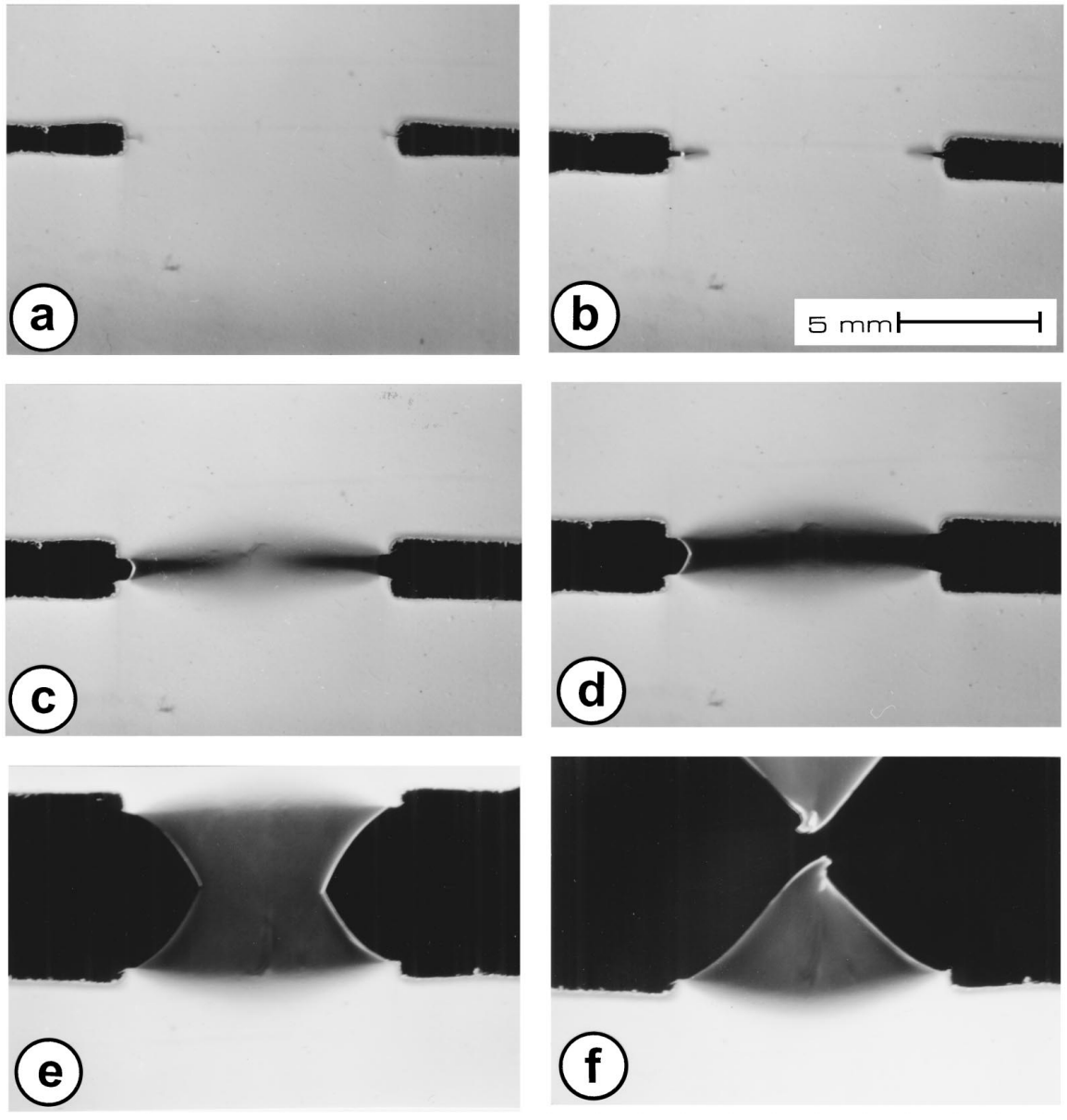


*Figure 2* Characteristic fracture behaviour of a m-iPP/EBR48(5 vol. %) DDENT specimen as recorded by light microscopy: (a) loading starts without visible marks, (b) end of quasi-elastic regime; notches open, (c) load maximum; visible plastic zone for each notch, (d) ligament yields fully, (e) stable crack propagation, (f) ultimate rupture.

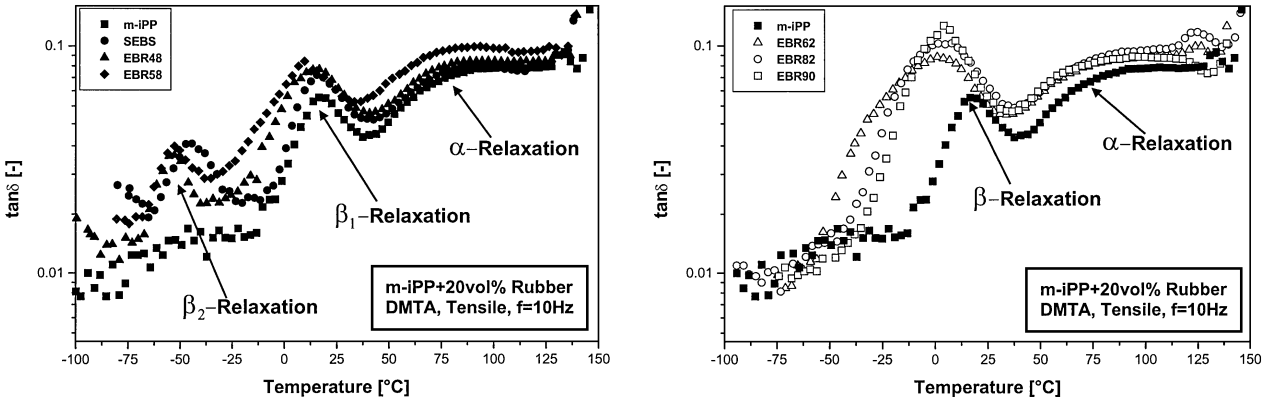


*Figure 3* DMTA spectra for the m-iPP+20 vol.%EBR binary blends (a) $\tan\delta - T$ for the immiscible blends, (b) $\tan\delta - T$ for the miscible blends.

and immiscible hereafter, according to DMTA results, and will also be considered separately in the discussion.

### 4.1.1. Immiscible blends

Fig. 3a shows the change of the mechanical loss factor, $\tan\delta(T)$, as a function of temperature. As seen on on the example of the 20 vol. % blends in EBR48 and −B58, apparently the $\tan\delta(T)$ traces exhibit the matrix and EBR relaxations, $\beta_1$ and $\beta_2$ respectively. The $\alpha$-relaxation, owing to intralamellar crystal re-orientation or interlamellar chain rearrangements of the PP matrix [17] is also visible.

It has been recently shown that in PP/EBR blends the $T_g$ of the elastomer is shifted towards lower temperatures. This effect is due to the mismatch in thermal expansion coefficients between the m-iPP and the dispersed elastomer and is thoroughly investigated in a recent work [18]. A negative $T_g$ shift can also be observed in the PP/EBR48 and PP/EBR58 blends [8].

SEM studies performed on cyclohexane etched cryogenic fracture surfaces of specimens of all binary blends confirmed the dispersed morphology of the m-iPP/EBR blends and thus correlate with the DMTA results. Fig. 4 shows the morphology of the immiscible blends of m-iPP with EBR48 and EBR58 after cyclohexane etching. At a high magnification the cavities which the rubber particles occupied before being selectively solved, can be well observed. The mean particle is about 1 $\mu$m.

### 4.1.2. Miscible blends

The $\tan\delta(T)$ traces of the blends with EBR62, −82, and −90, respectively, show partial miscibility with the PP resin, exhibiting a single, broad $T_g$ peak at $\approx$3.6 °C, as shown in Fig. 3b. Observe here that the $\beta$-relaxation width is decreasing with increasing 1-butene content of the EBR whereas the peak height follows exactly the opposite trend. m-iPP/EBR90(80/20 vol%) blend exhibits the narrowest distribution, the highest peak of all and thus the highest damping, too. This is a clear indication for full miscibility. Other researchers have shown that butene based (1-butene content >88 wt%) plastomers are fully miscible with the amorphous part of iPP. The interested reader is addressed to the related publications[7, 9–10].

Blends of high compatibility, i.e. m-iPP with EBR62, −82, and −90 respectively, delivered astonishing pictures of the binary blend morphology as can be seen in Fig. 5. The authors are not aware of the exact mechanisms which have driven the two components into such formations. EBR62 blend, in picture 5a, shows the typical formations of a co-continuous interpenetrating network (IPN) structure. In frame 5b, cavities the diameter of which is about 0.1 $\mu$m, indicate the presence of a nano-dispersed particle system. For the EBR90 blend, neither IPN nor cavity formations could be detected even at higher magnifications as seen in picture 5c.

The results from DMTA and SEM prove that an increase in the 1-butene content in EBR increases the compatibility between m-iPP and EBR, or even leads to miscible blends at high 1-butene contents. Based on the above results and literature information[7, 9–10] the following distinction between our systems with respect to blend miscibility, can be made:

Immiscible systems: PP with EBR48, EBR58

Partially miscible systems: PP with EBR62 and EBR82

Fully miscible system: PP with EBR90

## 4.2. Stiffness, strength and toughness parameters

The influence of blend composition on the stiffness and strength as well as on toughness properties is depicted in Fig. 6. Clearly, there is a significant decrease in both stiffness ($E$-moduli, Fig. 6a) and tensile yield strength (Fig. 6b) of all blends. As seen in Fig. 6a, $E$-moduli are quite sensitive to an increase in elastomer content, presenting the same linear decrease in almost all cases. Among the 5 vol.% blends, PP/EBR82 exhibits the highest $E$-modulus. Recall that the EBR82 is a highly crystalline grade. However, when mixed in higher quantities this advantage is lost. This is due probably to the partial miscibility of this rubber with m-iPP. It is to be noted that the lowest stiffness and strength data were shown by the m-iPP/EBR62 blends. EBR62 is completely amorphous and is partially miscible with the

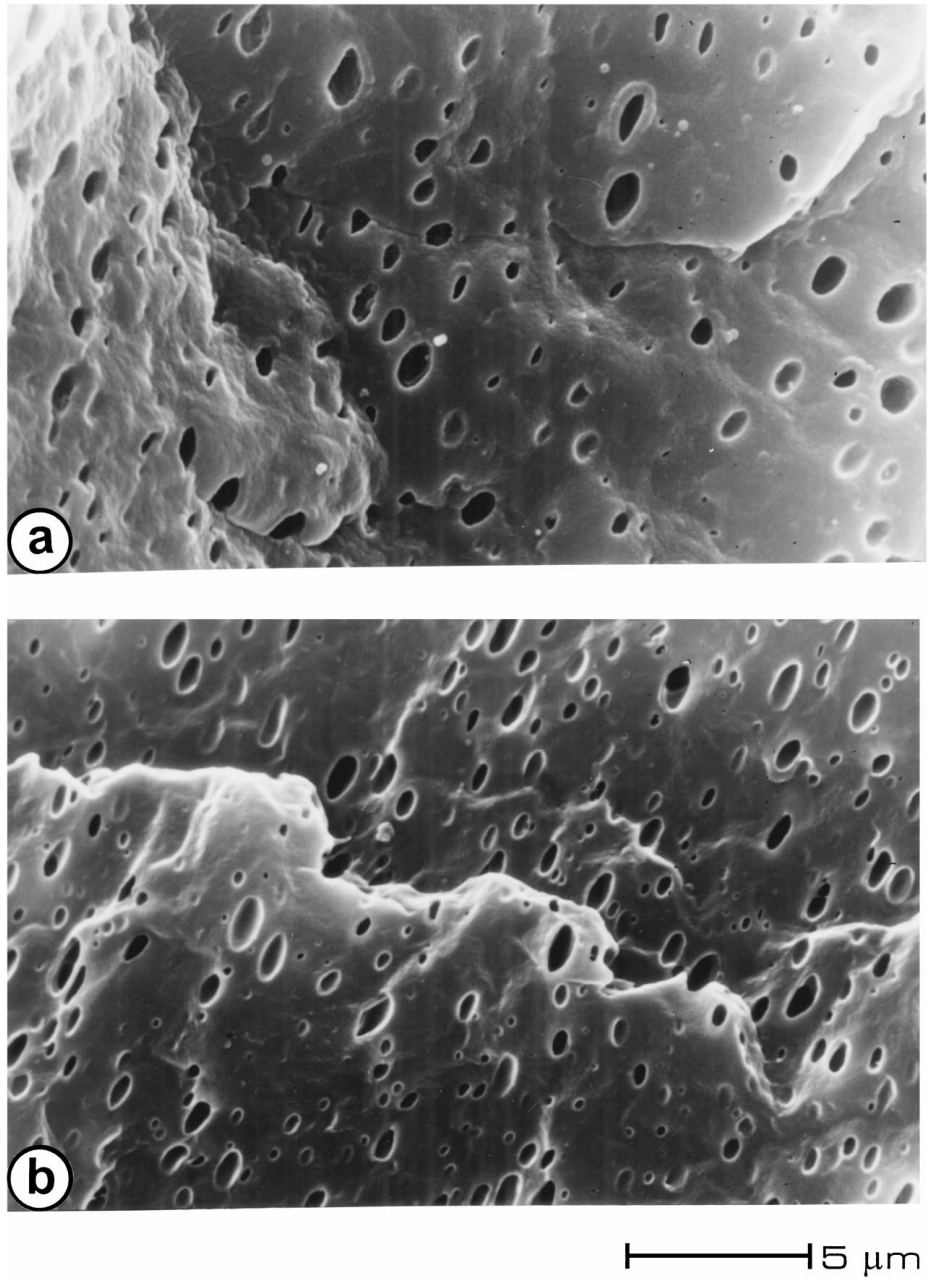


*Figure 4* SEM pictures of the cryo-fractured immiscible m-iPP/EBR blends, (a) 20 vol.%EBR48, (b) 20 vol.%EBR58.

m-iPP matrix so the low $E$-moduli are to be attributed to a synergy of both these effects.

The same trends are more or less valid for the yield strength data as seen in Fig. 6b. Again, EBR82 has the highest strengthening impact on the blend, however its high miscibility with m-iPP, results in a strength decrease, at EBR contents higher than 15 vol.%. m-iPP/EBR62 blends showed, once more, the poorest performance, due a synergistic effect of high miscibility and low rubber crystallinity.

Summarizing the stiffness/strength response of the PP/EBR blends, it can be stated, that rubber crystallinity and miscibility with the m-iPP matrix were identified as counteracting mechanisms.

Dynamic toughness response of the m-iPP/EBR binary blends as determined by means of Izod testing can be seen in the corresponding plots of Fig. 7. Izod toughness data at room temperature (see Fig. 7a) appear to be insensitive to the effect of rubber crystallinity as stated above. Instead, miscibility appears to play the key role in the impact toughness of the blends. It is well known that toughness is a morphology-related parameter in polymer blends, therefore miscibility which controlls morphology should be the dominant factor. A brittle to ductile transition is visible for the EBR48 and EBR58 blends at an EBR volume fraction of about 10%. Immiscible blends are much tougher in this case than all other types. m-iPP/EBR62 blends, exhibit the highest impact toughness of all fully and partially miscible blends. This is probably due to the effect that a dual-phase structure was also present in these blends [10, 11–15, 19], cf. Fig. 5b. EBR90, which as known is highly miscible with the PP matrix shows an inferior behaviour.

Izod tests where repeated for all blends at $-28\,^{\circ}\mathrm{C}$ but the data delivered did not give the expected trends for the miscible blends as seen in Fig. 7b. Recall here, the compatible blends present a unique $T_g$ peak at

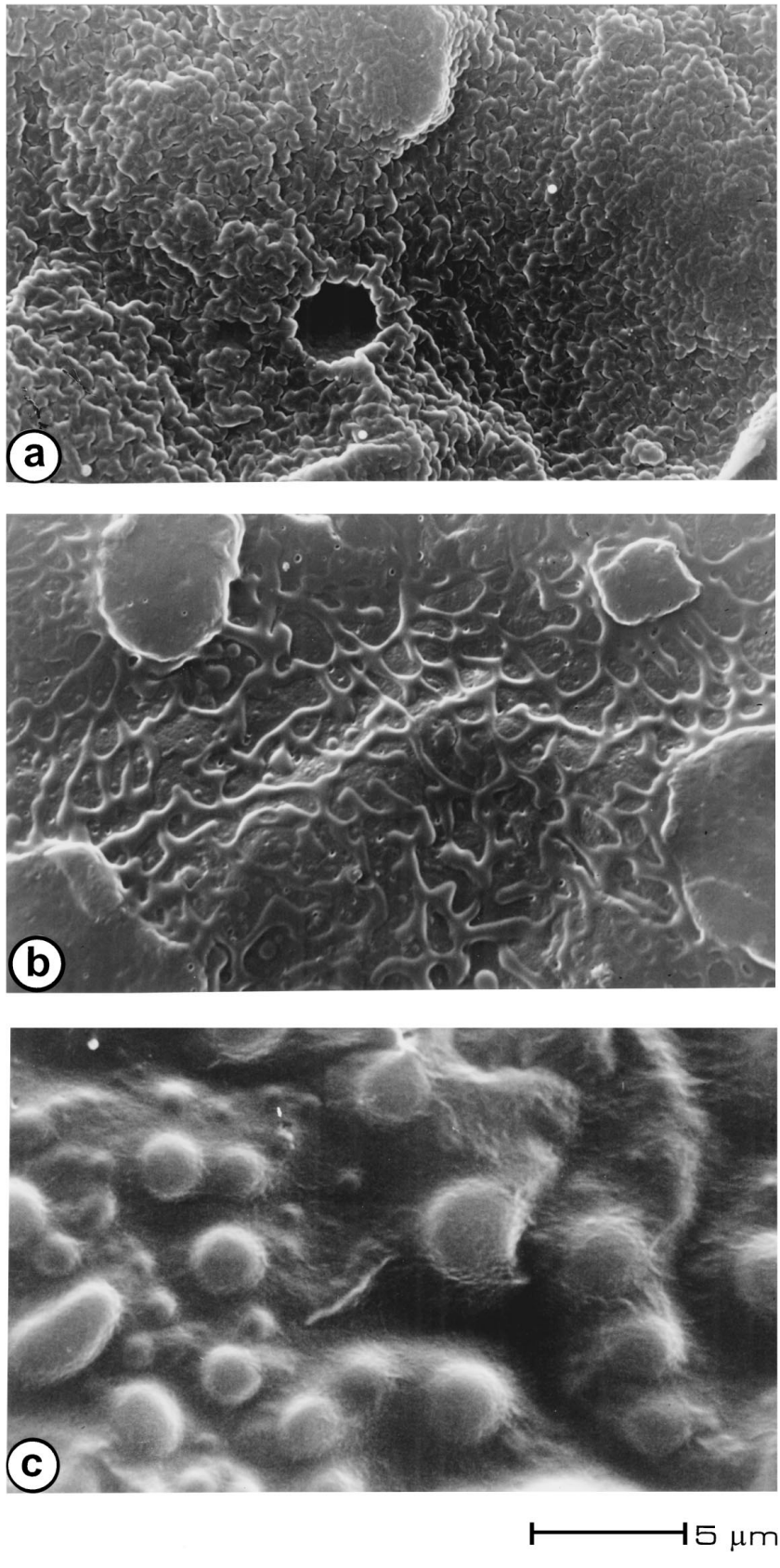


*Figure 5* SEM pictures of the cryo-fractured miscible m-iPP/EBR blends, (a) 20 vol.%EBR62, (b) 20 vol.%EBR82, (c) 20 vol.%EBR90.

≈3.6 °C (cf. Fig. 3b). Possibly, below this temperature the impact response becomes alike at all volume fractions. The results for the observed tendencies of the non miscible types of rubbers are in good concert with the results at room temperature. We would however like to point out here that peaks of the elastomer $T_g$ in these blends lay below −40 °C (cf. Fig. 3a). It can thus be concluded that impact response of the PP/EBR blends is sensitive to temperature change above the plastomer $T_g$.

Static toughness EWF data delivered very interesting results with respect to fracture toughness as they are presented in Fig. 8 and Table II. It appears that

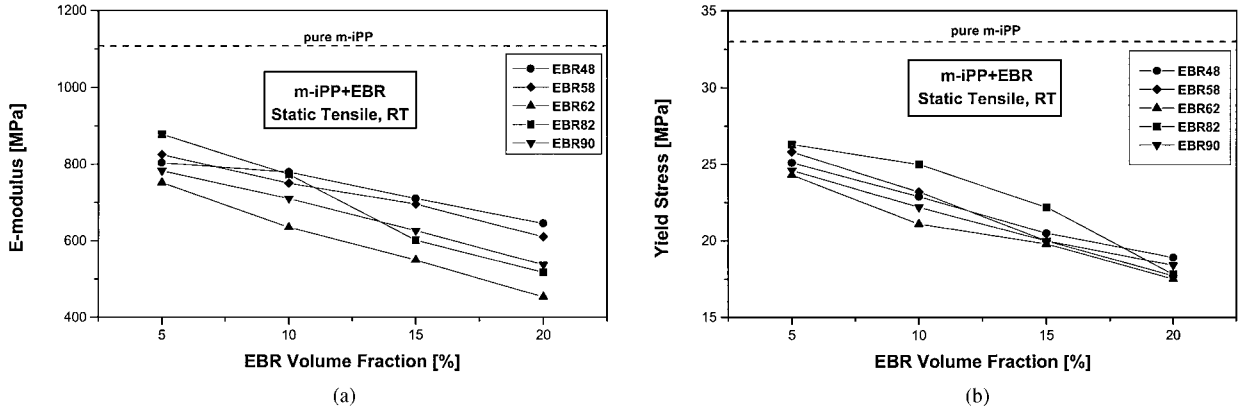


*Figure 6* Stiffness and strength properties of the m-iPP/EBR binary blends.

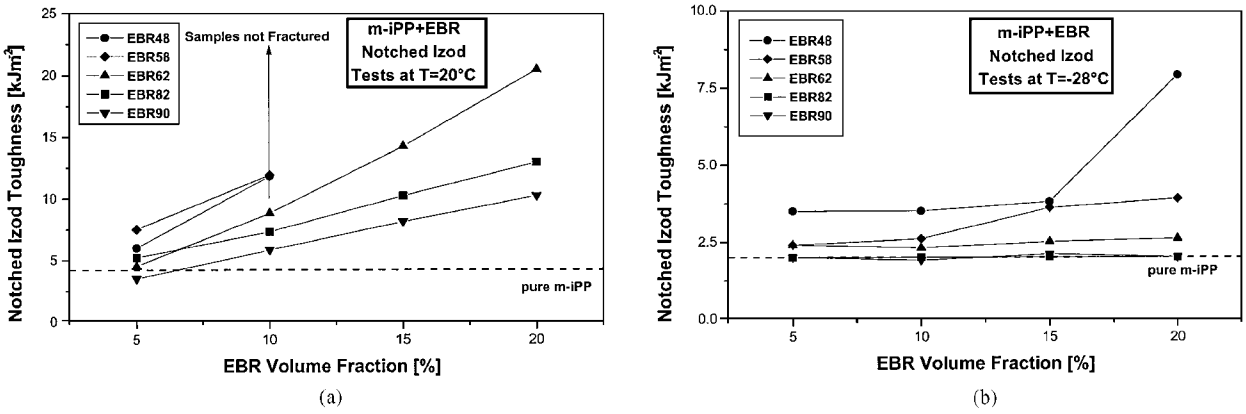


*Figure 7* Izod impact toughness properties of the m-iPP/EBR binary blends.

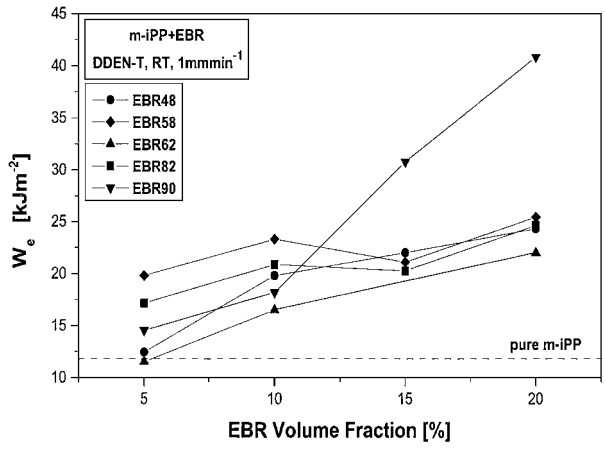


*Figure 8* Essential work of fracture data for the m-iPP/EBR blends.

in all cases, except for EBR90, the specific essential work of fracture passes through a local maximum. The exceptional performance of the EBR90 blends above a threshold of ca. 10 vol.% is to be attributed to the related phase morphology. This results in a system in which crack initiation resistance is quite high [20]. This effect was not reflected in the Izod impact properties. The authors would like to point out however that Izod toughness does not reflect a critical crack initiation parameter whereas the specific essential work of fracture does.

Plastic or non-essential work of fracture data ($\beta w_p$) are also presented in Table II. Clearly there is no significant change in the non-essential work with increasing EBR content. Interestingly, PP/EBR90 blends showed a linear reduction in $\beta w_p$ with increasing elastomer content. Attempt was made to explain this behaviour based on the morphology [20].

## 4.3. Fracture mode

Fig. 9 presents the difference in the plastic zone opacities observed for the compatible and non-compatible binary blends as captured during the fracture of the DDENT specimens. As seen on the example of a m-iPP/EBR58(85/15 vol%) specimen in Fig. 9a, all specimens of the immiscible blends exhibited an intense stress whitening in the plastic zone. This can be seen as the darker region in this picture since back lighting was used. Stress whitening effects are signs for the presence of mechanisms like cavitation and crazing in the matrix [3].

Plastic zone of the miscible blends on the other hand (m-iPP/EBR82, 85/15 vol%), remained more or less transparent during loading, (Fig. 9b). This is a clear hint for homogeneous plastic deformation.

### *4.3.1. Immiscible blends*

Fig. 10 presents the fracture surfaces of the incompatible blends. The fracture plane is dominated by fibrils and cavities. Matrix fibrillation is related to both cavitation and crazing, though hardly distinguishible. In order to establish the exact fracture mechanism with precision, a DDENT specimen of m-iPP/EBR58 (80/20 vol.%), was microtomed across the fracture

TABLE II Mechanical properties of the PP/EBR blends

| EBR type | EBR content (vol %) | Young's modulus (MPa) | Yield stress (MPa) | Specific essential work of fracture (kJ/m$^2$) | Specific plastic work, $\beta w_p$ [MJ/m$^3$] | Notched Izod impact strength at RT (kJ/m$^2$) | Notched Izod impact strength at $-28\,^\circ$C (kJ/m$^2$) |
|---|---|---|---|---|---|---|---|
| i-PP | — | 900 | 27.8 | 12 | — | 3.6 | 2.0 |
| EBR48 | 5 | 825 | 25.1 | 12.44 | 9.27 | 6.0 | 3.5 |
| | 10 | 779 | 22.9 | 19.79 | 8.8 | 11.8 | 3.5 |
| | 15 | 710 | 20.5 | 21.99 | 9.48 | n.b.[a] | 3.8 |
| | 20 | 645 | 18.9 | 24.29 | 9.35 | n.b.[a] | 7.9 |
| EBR58 | 5 | 804 | 25.8 | 19.8 | 9.98 | 7.5 | 2.4 |
| | 10 | 750 | 23.2 | 23.3 | 12.06 | 11.9 | 2.6 |
| | 15 | 695 | 20.0 | 21.07 | 10.28 | n.b.[a] | 3.6 |
| | 20 | 610 | 17.7 | 25.4 | 10.6 | n.b.[a] | 3.9 |
| EBR62 | 5 | 752 | 24.3 | 11.5 | 11.8 | 4.5 | 2.4 |
| | 10 | 635 | 21.1 | 16.49 | 11.19 | 8.8 | 2.3 |
| | 15 | 549 | 19.8 | ... | ... | 14.2 | 2.5 |
| | 20 | 453 | 17.5 | 21.97 | 11.05 | 20.4 | 2.6 |
| EBR82 | 5 | 878 | 26.3 | 17.15 | 9.19 | 5.2 | 2.0 |
| | 10 | 773 | 25.0 | 20.85 | 9.64 | 7.3 | 2.0 |
| | 15 | 601 | 22.2 | 20.24 | 10.38 | 10.2 | 2.0 |
| | 20 | 517 | 17.8 | 24.62 | 9.39 | 12.9 | 2.0 |
| EBR90 | 5 | 783 | 24.6 | 14.54 | 11.33 | 3.5 | 2.0 |
| | 10 | 710 | 22.0 | 18.17 | 10.71 | 5.8 | 1.9 |
| | 15 | 626 | 20.0 | 30.75 | 9.65 | 8.1 | 2.1 |
| | 20 | 537 | 18.4 | 40.83 | 8.84 | 10.2 | 2.0 |

[a]Sample did not break.

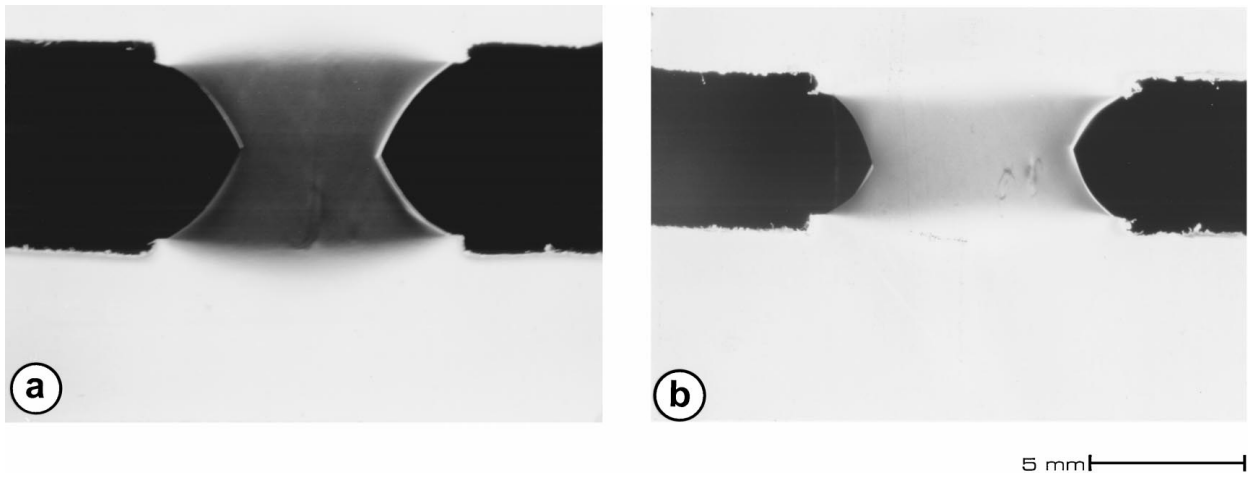


*Figure 9* Change in the opacity of the plastic zone of DDENT specimens as recorded by light microscopy: (a) m-iPP/EBR58(15 vol%), immiscible system ; (b) m-iPP/EBR82(15 vol%), partially miscible system.

plane and scanned in SEM. Fig. 11 depicts a SEM micrograph which shows cavities occupied by microfibrils. This microfibrillation of the elastomer particles, is likely to be the effect of crazing within the dispersed elastomer particles. Matrix cavities initiate and deform, due to local stress concentrations around the elastomer particles. During this procedure, the elastomer particles deform also, as they are still attached on the PP matrix. Picture in Fig. 10 provides an indirect proof of the good adhesion between matrix and elastomer particles [18]. Hence, the fracture mechanism of the incompatible blends can be summarized as: matrix cavitation and crazing initiated by the elastomer particles, followed by plastic deformation of the matrix.

### 4.3.2. Miscible blends

All three types of the partially-miscible PP/EBR blends exhibited a similar response to fracture. As seen in Fig. 12, the governing fracture mechanism for these materials is ductile tearing at a smaller or a larger scale, depending on the EWF related toughness of these blends. By comparing the specific EWF data sequence in Table II, it can be stated:

$$w_e^{EBR62} < w_e^{EBR82} < w_e^{EBR90}$$

This is exactly the trend the corresponding fracture planes reflect. Recall the surface dependence of the $w_e$ data.

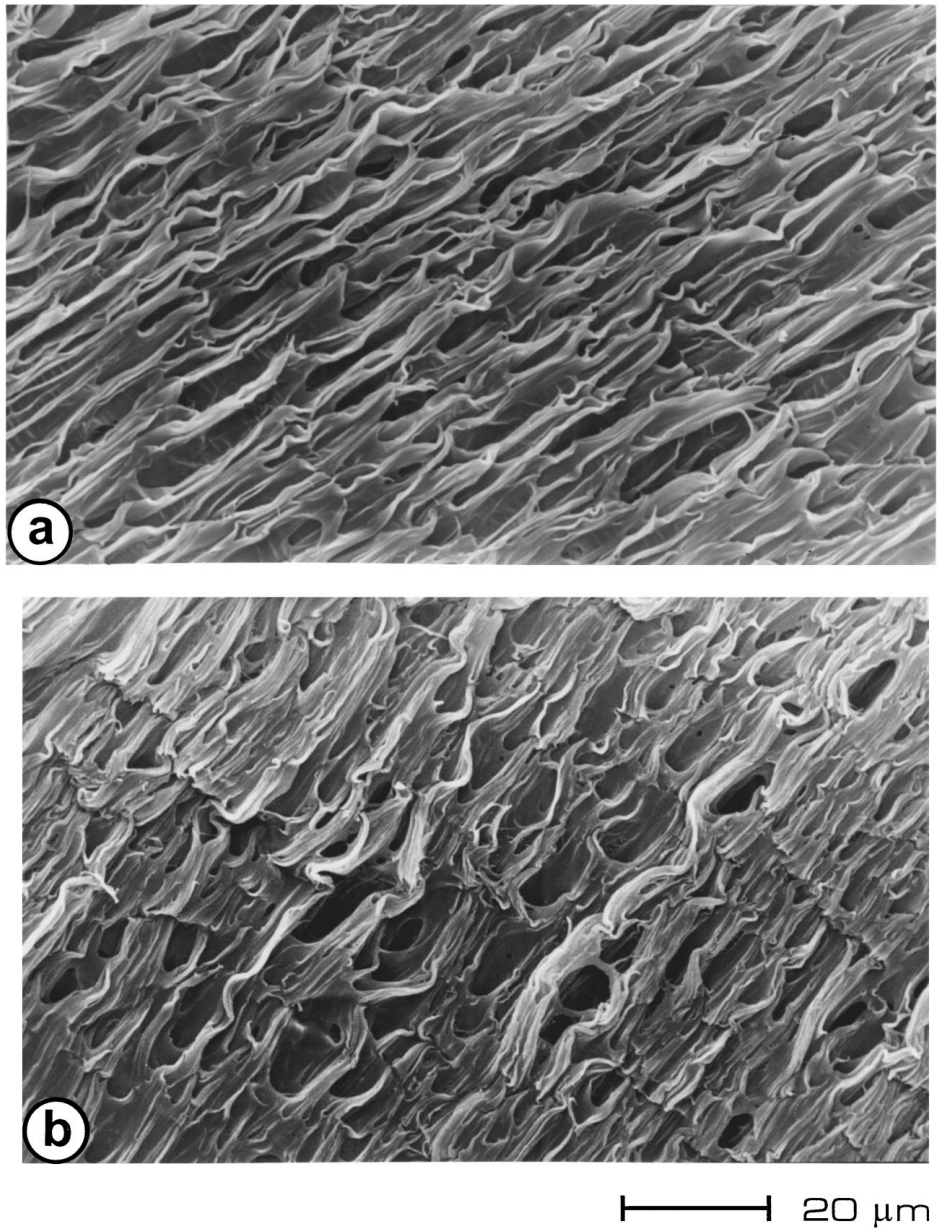


*Figure 10* Fracture surfaces of DDENT specimens of the immiscible m-iPP/EBR blends, (a) (20 vol%)EBR48, (b) (20 vol%)EBR58.

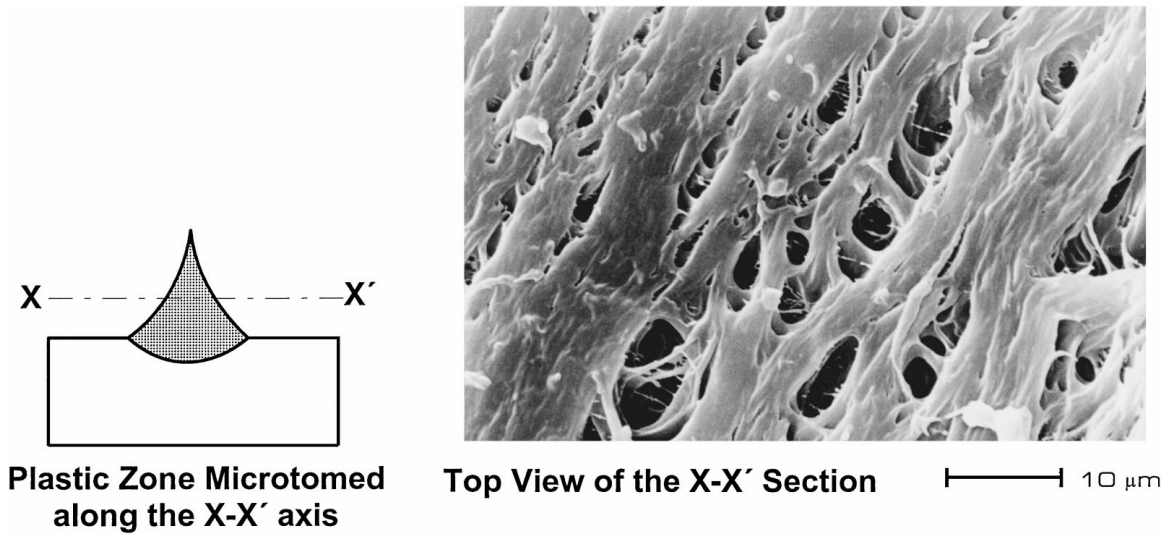


*Figure 11* Cavitation as seen on a SEM picture taken on the transversely microtomed plastic zone of a m-iPP/EBR58(20 vol%) DDENT specimen.

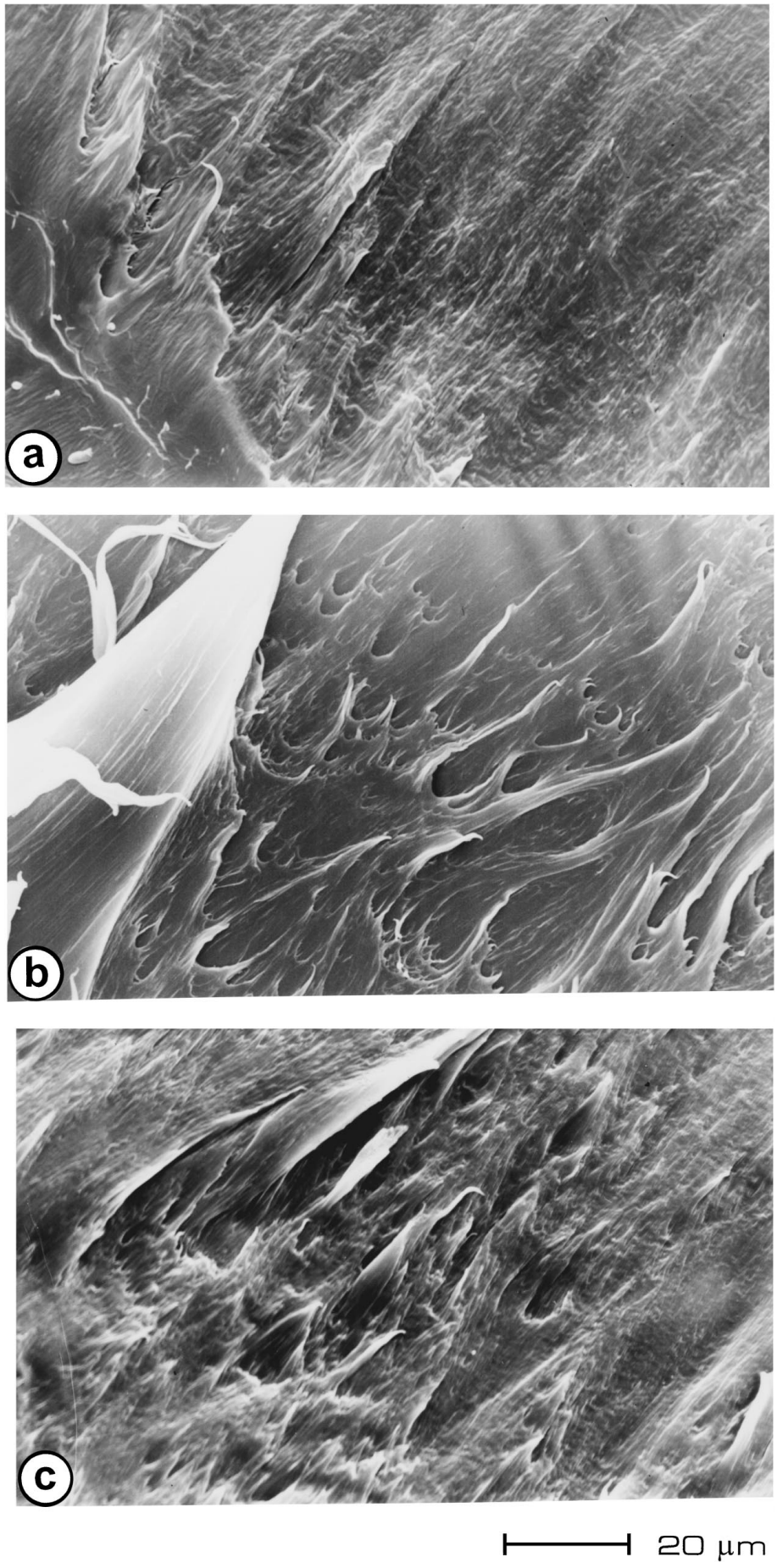


*Figure 12* Fracture surfaces of DDENT specimens of the miscible m-iPP/EBR blends, (a) (20 vol%)EBR62, (b) (20 vol%)EBR82, (c) (20 vol%)EBR90.

## 5. Conclusions

Based on the above study performed on i-PP/EBR blends, the following conclusions can be drawn:

### 5.1. Morphology

It was found that the increasing 1-butene content in EBR rubbers favours the miscibility with the m-iPP matrix especially when the 1-butene content of the EBR rubber exceeds 58 wt%. Total miscibility was confirmed for EBR systems where 1-butene content is 90 wt%.

### 5.2. Stiffness and strength

Increasing miscibility has a negative effect on the *E*-modulus and yield strength at EBR volume fractions above ca. 10%. Elastomer crystallinity in synergy with good miscibility enhances stiffness only at volume fractions below 10%.

### 5.3. Dynamic impact toughness

Immiscible PP/EBR blends have shown superior notched Izod impact strength. Increasing EBR miscibility resulted in inferior impact behaviour. Non-miscible EBRs allow several energy dissipation mechanisms to take place during fracture thus enhancing the impact toughness, in contrast to the miscible ones which exhibit only plastic deformation.

### 5.4. Essential work of fracture

The specific essential work of fracture data reflected a sensitivity against increasing elastomer content (i.e. decreasing interparticle distance) for almost all blends. In the case of the EBR90 blends, an extraordinary high crack initiation resistance was observed above 10 vol%. This is related to a peculiar morphology [18,20].

### 5.5. Failure mode

Fracture surface morphologies were in perfect agreement with the specific essential work of fracture data. Cavitation, crazing and shear yielding for the incompatible blends were confirmed to be the controlling fracture mechanisms associated with large plastic zones. On the other hand, plastic deformation followed by ductile tearing occurred in the miscible PP/EBR blends, where a confined plastic zone size was found.

## References


1. E. MARTUSCELLI, in "Polypropylene: Structure, Blends and Composites," Vol. 2, edited by J. Karger-Kocsis (Chapman and Hall, London, 1995) p. 95.
2. P. GALLI, J. C. HAYLOCK and T. SIMONAZZI, in "Polypropylene: Structure, Blends and Composites," Vol. 2, edited by J. Karger-Kocsis (Chapman and Hall, London, 1995) p. 1.
3. D. E. MOUZAKIS, F. STRICKER, R. MÜLHAUPT and J. KARGER-KOCSIS, *J. Mater. Sci.* **33** (1998) 2551.
4. F. STRICKER, Y. THOMANN, and R. MÜLHAUPT, *J. Appl. Poly. Sci.* **68** (1998) 1891.
5. R. MÜLHAUPT, in "Polypropylene: An A-Z reference," edited by J. Karger-Kocsis (Kluwer Publ., Dordrecht 1999) p. 454.
6. S. BENSASON, J. MINICK, A. MOET, S. P. CHUM, A. HILTNER and E. J. BAER, *J. Polym. Sci. Polym. Phys.* **34** (1996) 1301.
7. M. YAMAGUCHI, H. MIYATA and K. H. NITTA, *J. Appl. Polym. Sci.* **62** (1996) 87.
8. K. NITTA, K. OKAMOTO and M. YAMAGUCHI, *Polymer* **39** (1998) 53.
9. Y. THOMANN, J. SUHM, R. THOMANN, G. BAR, R.-D. MAIER and R. MÜLHAUPT, *Macromolecules* **31** (1998) 5441.
10. D. MÄDER, Y. THOMANN, J. SUHM and R. MÜLHAUPT, *J. Appl. Polym. Sci.* **74** (1999) 838.
11. K. B. BROBERG, *Mech. Phys. Solids* **23** (1975) 215.
12. Y. W. MAI and B. COTTERELL, *Int. J. Fracture* **32** (1986) 105.
13. O. F. YAP, Y. W. MAI and B. COTTERELL, *J. Mater. Sci.* **18** (1983) 657.
14. ESIS 1997, European Structural Integrity Society TC-4 group, Testing Protocol for Essential Work of Fracture.
15. A. E. WOODWARD, "Atlas of Polymer Morphology" (Hanser, München, 1989) p. 305.
16. H. A. SCHNEIDER, in "Polymeric Materials Encyclopedia," Vol. 4, edited by J. C. Salomone (CRC Press, Boca Raton, 1996) p. 2777.
17. Y. YOKOYAMA and T. RICCO, *Polymer* **39** (1998) 3675 .
18. D. MÄDER, M. BRUCH, R.-D. MAIER, F. STRICKER and R. MÜLHAUPT, *Macromolecules* **32** (1999) 1252.
19. J. SUHM, M. J. SCHNEIDER and R. MÜLHAUPT, *J. Mol. Cat. (Part A)* **128** (1998) 215.
20. J. KARGER-KOCSIS, *J. Macromol. Sci. Phys.* **B38** (1999) 645.



*Received 24 December 1998*
*and accepted 11 August 1999*